machines

MDPI

Article

A Walking Trajectory Tracking Control Based on Uncertainties Estimation for a Drilling Robot for Rockburst Prevention

Jinheng Gu [1,2], Shicheng He [1,2], Jianbo Dai [1,2], Dong Wei [1,2], Haifeng Yan [1,2], Chao Tan [1,2], Zhongbin Wang [1,2] and Lei Si [1,2,*]

[1] School of Mechatronic Engineering, China University of Mining and Technology, Xuzhou 221116, China; gujinheng@126.com (J.G.); jianbodai@126.com (J.D.); weidongcmee@cumt.edu.cn (D.W.); yanhaifeng@cumt.edu.cn (H.Y.); tccadcumt@126.com (C.T.)

[2] Jiangsu Key Laboratory of Mine Mechanical and Electrical Equipment, China University of Mining and Technology, Xuzhou 221116, China

* Correspondence: lei.si@cumt.edu.cn

Abstract: A walking trajectory tracking control approach for a walking electrohydraulic control system is developed to reduce the walking trajectory tracking deviation and enhance robustness. The model uncertainties are estimated by a designed state observer. A saturation function is used to attenuate sliding mode chattering in the designed sliding mode controller. Additionally, a walking trajectory tracking control strategy is proposed to improve the walking trajectory tracking performance in terms of response time, tracking precision, and robustness, including walking longitudinal and lateral trajectory tracking controllers. Finally, simulation and experimental results are employed to verify the trajectory tracking performance and observability of the model uncertainties. The results testify that the proposed approach is better than other comparative methods, and the longitudinal and lateral trajectory tracking average absolute errors are controlled in 10.23 mm and 22.34 mm, respectively, thereby improving the walking trajectory tracking performance of the walking electrohydraulic control system for the coal mine drilling robot for rockburst prevention.

Keywords: walking trajectory tracking control; state observer; sliding mode control; walking electrohydraulic control system; coal mine drilling robot for rockburst prevention

Citation: Gu, J.; He, S.; Dai, J.; Wei, D.; Yan, H.; Tan, C.; Wang, Z.; Si, L. A Walking Trajectory Tracking Control Based on Uncertainties Estimation for a Drilling Robot for Rockburst Prevention. *Machines* **2024**, *12*, 298. https://doi.org/10.3390/machines12050298

Academic Editors: Dan Zhang and Manuel F. Silva

Received: 31 March 2024
Revised: 23 April 2024
Accepted: 26 April 2024
Published: 28 April 2024

1. Introduction

The borehole pressure relief method has become an effective way to prevent coal mine rockburst in China, which can reduce the impact of dynamic disasters for deep coal mining [1–3]. During this period, moving the drilling robot to the target position is the precondition for realizing an effective borehole [4,5]. Furthermore, the accurate walking trajectory tracking control directly determines whether the drilling robot can move to the target position. In the moving process of the drilling robot, the walking electrohydraulic control system (WECS) enables the drilling rig to move, which is commonly driven by two hydraulic motors. The efficient operation of two hydraulic motors directly affects the walking position and deviation of the drilling rig. Nevertheless, the walking trajectory tracking control accuracy and stability of the walking system are not easy to obtain because of the nonlinear characteristics. Simultaneously, different walking conditions such as the coal mine roadway surface are uneven and external disturbances, leading to walking trajectory deviations from the expected path and even causing collision accidents.

To overcome the trajectory tracking control challenge, a variety of studies to improve the control performance have been conducted for the trajectory tracking control, e.g., speed control to track reference trajectory [6], speed predictive control [7], active disturbance rejection control [8,9], sliding mode control for path tracking [10,11], and adaptive control [12,13]. From these studies, the accurate trajectory tracking control behavior cannot be easily guaranteed in the presence of uncertainties or external disturbances, especially for

the coal mine drilling robot for rockburst prevention (CMDR). Furthermore, sliding mode control (SMC) is selected as an effective control method for achieving expected tracking control performance [14,15], and the chattering phenomenon of the SMC can be reduced by the saturation function [16,17]. A sliding mode controller based on a high-gain observer was designed to improve the control performance [18]. A sliding mode observer-based controller is designed to ensure highly accurate tracking control characteristics [19]. A sliding mode controller is designed to improve the control precision and attenuate the disturbances, including model uncertainties and external disturbances [20]. Nevertheless, the relevant application of the SMC method in the WECS for the CMDR is still scarce. Moreover, the estimation of model uncertainties and disturbances are lacked for the trajectory tracking control of the WECS. Accordingly, a walking trajectory tracking control scheme urgently needs to be proposed to enhance the system performance of the WECS.

To reduce the adverse effects of model uncertainties and disturbances, some observer-based control methods have been applied to reduce the tracking deviation, e.g., a fuzzy observer-based composite nonlinear controller for trajectory tracking is presented to improve the tracking performance [21]. An extended state observer-based sliding mode controller is developed to estimate the lumped uncertainty and achieve robust tracking performance [22]. An unscented Kalman filter is used to estimate detection error, and the proposed trajectory tracking control strategy can effectively achieve target trajectory scheduling with a limited adjustment period [23]. A robust adaptive neural network trained with the integral sliding mode is presented to enhance the path-tracking performance, which has the capacity for state estimation and auxiliary control inputs [24]. A nonlinear disturbance observer is designed to estimate the system states, and a sliding mode controller is designed to improve the control efficiency and response characteristics [25]. An adaptive robust controller and a state feedback controller are proposed to effectively handle parametric uncertainties and uncertain nonlinearities, which can reveal the connection between achievable performances and control parameters [26]. Consequently, the model uncertainties and disturbances need to be estimated in the trajectory tracking control to eliminate tracking deviations in the regulation motion. However, there is still no effective way to handle the multiple uncertainties and disturbances in the WECS. Moreover, the mixture effects of model uncertainties and external disturbances in the WECS may bring more challenges for walking trajectory tracking control.

To exploit an adapted controller for the electrohydraulic system, sliding mode control and its extended methods are known as efficient nonlinear control algorithms for an engineering system. The observer-based tracking controller is designed to improve system response characteristics and has been applied in many systems [27–29]. Although many previous studies have solved the tracking control problem, the system characteristics also suffer in various working conditions because of parameter perturbations. In designing a controller for the WECS, when the walking trajectory loop experiences external disturbances, such as roadway excitation load and parameter mismatches, a state observer and control strategy are crucial to guarantee accurate trajectory tracking control and robustness. In the field of electrohydraulic control, a disturbance observer-based control is developed to estimate the uncertainties and guarantee the response performance [30,31]. Furthermore, the state estimator and SMC-based method are designed to enhance the system response characteristics [32,33]. Therefore, a feasible controller with an accurate trajectory tracking control needs to be applied in the walking motion of the CMDR. However, the accurate trajectory tracking of WECS is to cover some indeterminate parameters. Furthermore, the interference between these parameters may affect the controller regulating process.

Motivated by the previous analysis, a walking trajectory tracking control method for the WECS is presented to improve performance. The main contributions can be stated as:

(1) A coupled model is presented to analyze walking characteristics for the WECS, in which combing a walking motion model and an electrohydraulic control model to decompose the walking trajectory tracking control law, thereby improving the tracking control efficiency of the WECS.

(2) Model uncertainties and external disturbances are observed by a state observer for the WECS based on an improved radial basis function. Additionally, a proper selection of the saturation function could reduce the chattering phenomenon and enhance the tracking capability of the WECS.

(3) Compared with other existing control approaches, the presented control scheme for the WECS has a better performance in both walking longitudinal and lateral trajectory tracking control, which reduces the walking trajectory tracking average absolute error.

The remainder of this study is organized as follows. The configuration description and mathematical model of the WECS including the walking motion model and electrohydraulic control model are shown in Section 2. The state observer, walking longitudinal, and lateral trajectory tracking controller are designed in Section 3, and the walking trajectory tracking control strategy is proposed. In Section 4, simulations and experiments are conducted and compared with other existing methods. Conclusions are drawn in Section 5.

2. Walking Electrohydraulic Control System Analysis

2.1. Walking Process Description and Analysis

The WECS of the CMDR makes the tracked chassis move to achieve linear and steering walking, which is determined by the differential control of the left and right hydraulic motors. For the WECS, the linear and steering walking are controlled by two hydraulic motors that are installed on the left and right sides of the tracked chassis. When the drilling robot travels in a straight line, it is necessary to ensure that the left and right hydraulic motors output the same speed. And the steering walking relies on the differential speed control. These left and right hydraulic motors are coordinated and controlled by the electrohydraulic control system to achieve stable and accurate speed regulation, and the schematic diagram of a WECS of the CMDR is shown in Figure 1.

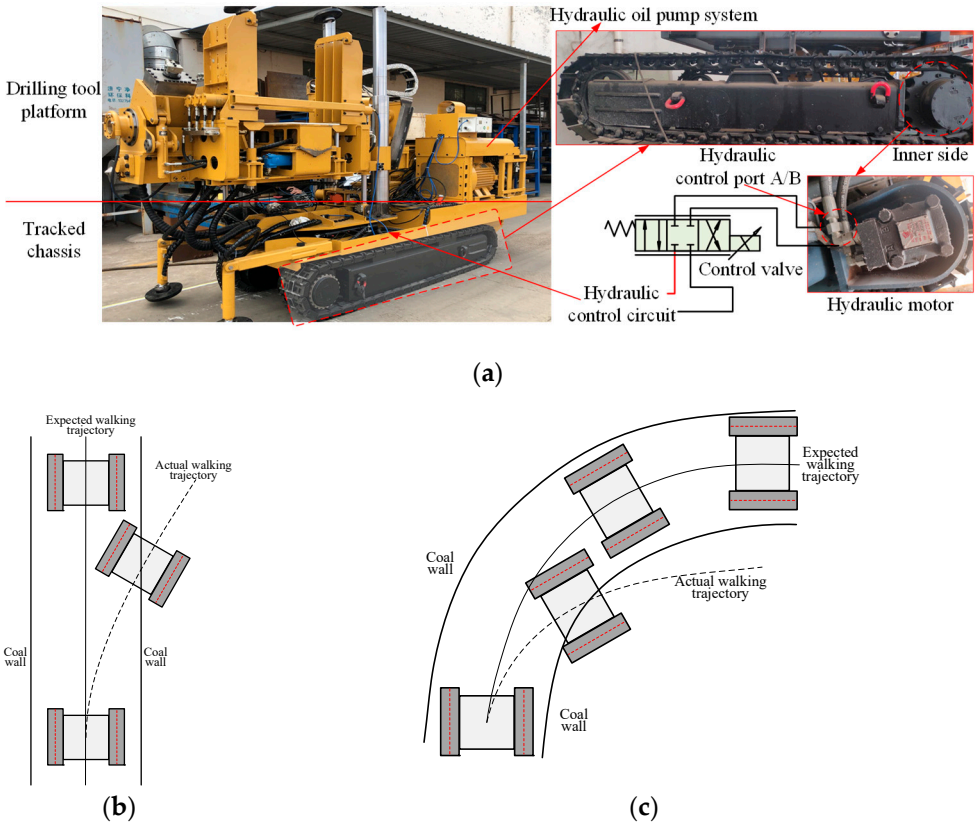

Figure 1. The schematic diagram of a WECS: (**a**) the main components in a WECS; (**b**) schematic diagram for straight walking trajectory; (**c**) schematic diagram for steering walking trajectory. Note: red line represents a partial schematic diagram.

For the WECS, the straight and steering walking trajectory is regulated by the speed control of the left and right hydraulic motors, using the speed sensors as feedback input, the adjustment values are calculated and transmitted to the electrohydraulic proportional directional valves by the controller, generating different walking conditions of the coal mine robot for rockburst prevention. As a result, a speed sensor information continuous acquisition and electrohydraulic control system with proportional directional valves based on a WECS is proposed, as shown in Figure 2. The left and right hydraulic motors are separately controlled by proportional directional valves. Additionally, the controller and the host computer are utilized to obtain the speed signal, the attitude signal of the CMDR, the output electrohydraulic proportional directional valve control signal, and control parameters debugging.

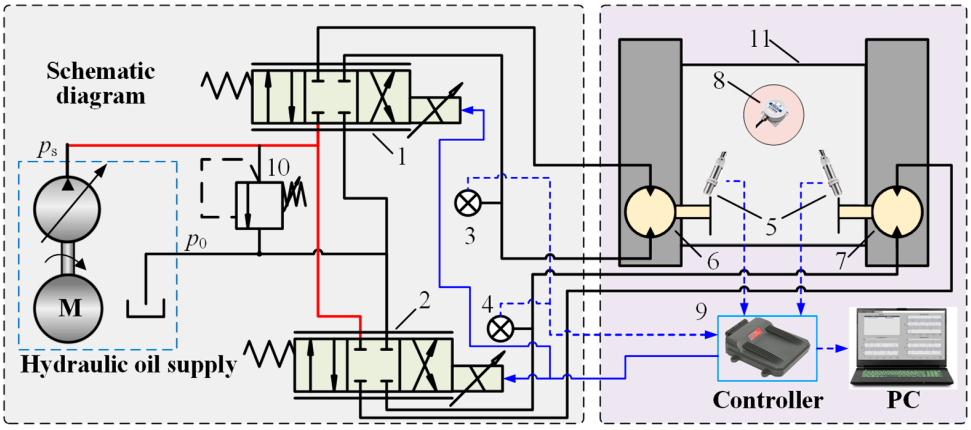

Figure 2. WECS principle. Notes: 1, 2—electrohydraulic proportional directional valve; 3, 4—pressure sensor; 5—speed sensor; 6—left hydraulic motor; 7—right hydraulic motor; 8—attitude sensor; 9—controller; 10—safety relief valve; 11—simplified model of the tracked chassis; red line represents high-pressure hydraulic pipeline; blue line represents control signal flow; blue dotted line represents sensor signal flow.

2.2. Walking Model Analysis

Referring to Figure 1, the straight and steering walking trajectory is regulated by the speed control of the left and right hydraulic motors. Taking the forward direction of the tracked chassis as the x direction, the yaw motion direction of the tracked chassis as y direction, and the geometric center of the tracked chassis as the point of o, OXY is the inertial coordinate system fixed to the coal roadway and oxy is the implicated coordinate system fixed to the tracked chassis. Furthermore, the walking model of the tracked chassis can be described in Figure 3.

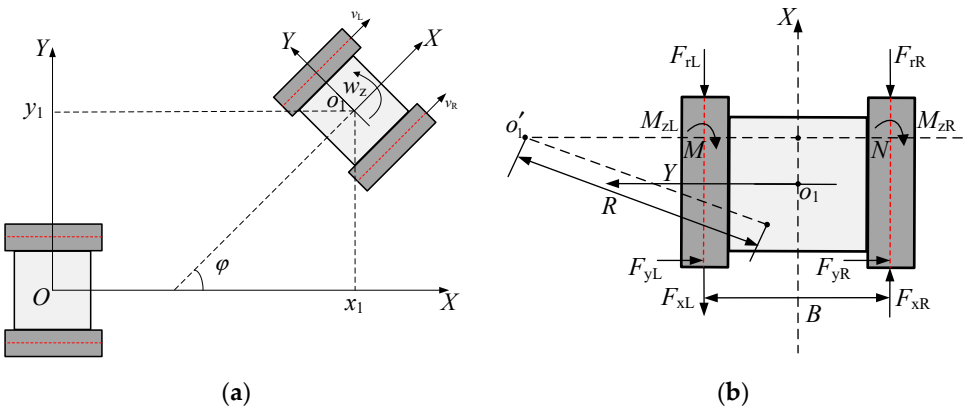

(**a**) (**b**)

Figure 3. The schematic diagram of a walking model: (**a**) the kinematics model of a tracked chassis; (**b**) the dynamic model of a tracked chassis. Notes: black and red dotted lines represent indicator lines.

Furthermore, the walking function is achieved by adjusting the speed difference between the left and right hydraulic motors. Assuming that the state of the tracked chassis is (x_0, y_0, φ_0), and the kinematic model can be described as:

$$\begin{bmatrix} \dot{x}_0 \\ \dot{y}_0 \\ \dot{\varphi} \end{bmatrix} = \begin{bmatrix} \sin\varphi & \cos\varphi & 0 \\ -\cos\varphi & \sin\varphi & 0 \\ 0 & 0 & 1 \end{bmatrix} \begin{bmatrix} v_x \\ v_y \\ w_z \end{bmatrix} \tag{1}$$

where φ is the heading angle of the tracked chassis, w_z is the yaw angle velocity of the tracked chassis.

Based on the kinematic model of Equation (1), combined with the model establishment process in the study [34], the Equation (1) can be rewritten as:

$$\begin{bmatrix} \dot{x}_0 \\ \dot{y}_0 \\ \dot{\varphi} \end{bmatrix} = \begin{bmatrix} \sin\varphi & \cos\varphi & 0 \\ -\cos\varphi & \sin\varphi & 0 \\ 0 & 0 & 1 \end{bmatrix} \begin{bmatrix} \frac{y'_{\mathrm{L}} v_{\mathrm{jH}} - y'_{\mathrm{H}} v_{\mathrm{jL}}}{y'_{\mathrm{L}} - y'_{\mathrm{H}}} y'_{\mathrm{o}} \\ \frac{v_{\mathrm{jL}} - v_{\mathrm{jH}}}{y'_{\mathrm{L}} - y'_{\mathrm{H}}} x'_0 \\ -\frac{v_{\mathrm{jL}} - v_{\mathrm{jH}}}{y'_{\mathrm{L}} - y'_{\mathrm{H}}} \end{bmatrix} \tag{2}$$

$$\begin{cases} y'_{\mathrm{L}} = \frac{v_x - v_{\mathrm{jL}}}{w_z}; & y'_{\mathrm{H}} = \frac{v_x - v_{\mathrm{jH}}}{w_z} \\ y'_0 = \frac{v_x}{w_z}; & x'_{\mathrm{L}} = x'_{\mathrm{H}} = x'_0 = -\frac{v_y}{w_z} \end{cases} \tag{3}$$

where $o'(x'_{\mathrm{o}}, y'_{\mathrm{o}})$ is the instantaneous turning center of tracked vehicles in the inertial coordinate system; $o_{\mathrm{L}}(x'_{\mathrm{L}}, y'_{\mathrm{L}})$ is the instantaneous turning center of the low-speed side track in the inertial coordinate system; $o_{\mathrm{H}}(x'_{\mathrm{H}}, y'_{\mathrm{H}})$ is the instantaneous turning center of the high-speed side track in the inertial coordinate system; v_{jL}, v_{jH} are the winding speeds of the low-speed side and high-speed side tracks, respectively.

Based on Figure 3b, the dynamic model for the tracked chassis can be described as:

$$\begin{cases} F_{\mathrm{Cy}} - \left(F_{\mathrm{yL}} + F_{\mathrm{yR}}\right) - m\ddot{x}_o = 0 \\ F_{\mathrm{xR}} - F_{\mathrm{xL}} - \left(F_{\mathrm{rL}} + F_{\mathrm{rR}}\right) - F_{\mathrm{Cx}} - \delta m\ddot{y}_o = 0 \\ \left(-F_{\mathrm{xR}} + F_{\mathrm{xL}} + F_{\mathrm{rL}} + F_{\mathrm{rR}}\right)\frac{B}{2} + \left(F_{\mathrm{Cy}} x_C + F_{\mathrm{Cx}} y_C\right) \\ -M_C - J\ddot{\varphi} = 0 \\ M_C = M_{\mathrm{CL}} + M_{\mathrm{CR}} \end{cases} \tag{4}$$

where m is the mass of the drilling robot; δ is the coefficient of the rotational mass for the drilling robot; M_C is total steering resistance moment; M_{CL}, M_{CR} are the left and right tracks' steering resistance moment, respectively; J is inertia moment; F_{C} (F_{Cx}, F_{Cy}) is the centrifugal force; B is the track width between the left and right tracks.

Assuming that the steering speed is constant and the expected longitudinal speed and the structural parameters are given, the driven force can be described as:

$$\begin{cases} F_{\mathrm{xR}} = F_{\mathrm{rR}} - \frac{1}{B}\left(F_{\mathrm{Cy}} x_C + F_{\mathrm{Cx}} y_C - M_C\right) + \frac{1}{2} F_{\mathrm{Cx}} \\ F_{\mathrm{xL}} = -F_{\mathrm{rL}} - \frac{1}{B}\left(F_{\mathrm{Cy}} x_C + F_{\mathrm{Cx}} y_C - M_C\right) - \frac{1}{2} F_{\mathrm{Cx}} \\ \lambda_C = \frac{L F_{\mathrm{Cy}}}{2\mu m g} + x_C \end{cases} \tag{5}$$

where μ is the resistance coefficient; L is the longitudinal length of the tracked chassis; g is the gravitational acceleration.

2.3. Mathematical Model of the Valve-Controlled Motor

For the WECS, the left and right hydraulic motors have the same motion function to support the adjustment of the walking of CMDR. As the walking trajectory tracking control condition for enhancing controllability, the designed control strategy must generate dynamic response performance [35,36]. The straight and steering walking of the WECS changes with the speed difference of the left and right hydraulic motors, which are controlled by the electrohydraulic proportional directional valves, i.e., the valve-controlled

motor speed control system. Therefore, the mathematical model of the hydraulic motor can be described as:

$$\begin{cases} q_{\mathrm{L}} = K_{\mathrm{q}} x_{\mathrm{mv}} - K_{\mathrm{c}} p_{\mathrm{L}} \\ q_{\mathrm{L}} = D_{\mathrm{m}} \dot{\theta}_{\mathrm{m}} + \frac{V_{\mathrm{t}}}{4\beta_{\mathrm{e}}} \dot{p}_{\mathrm{L}} + C_{\mathrm{m}} p_{\mathrm{L}} \\ D_{\mathrm{m}} p_{\mathrm{L}} = J_{\mathrm{m}} \ddot{\theta}_{\mathrm{m}} + B_{\mathrm{m}} \dot{\theta}_{\mathrm{m}} + G_{\mathrm{m}} \theta_{\mathrm{m}} + T_{\mathrm{m}} \end{cases} \tag{6}$$

where p_{L}, q_{L} represent the load pressure and flow, respectively; K_{q}, K_{c} represent the flow and flow–pressure gain coefficient, respectively; D_{m}, θ_{m} represent the displacement volume and angular displacement of the hydraulic motor, V_{t} represents the total volume of the hydraulic motor; β_{e} represents the bulk modulus of hydraulic oil; C_{m} represents the total leakage coefficient; J_{m}, B_{m}, G_{m}, T_{m} represent the inertia moment, viscous damping coefficient, torsion spring stiffness, and load torque of the hydraulic motor, respectively.

We assume the relationship between the input control signal and proportional directional valve spool displacement is given as:

$$x_{\mathrm{mv}} = k_{\mathrm{mv}} u_{\mathrm{mv}} \tag{7}$$

where k_{mv} is the gain coefficient between the valve spool displacement x_{mv} and control input signal u_{mv} for the hydraulic motor.

Simultaneously, with Equations (6) and (7), the transfer function between the x_{mv} and θ_{m} can be obtained as:

$$\frac{\theta_{\mathrm{m}}}{x_{\mathrm{mv}}} = \frac{K_{\mathrm{q}}/D_{\mathrm{m}}}{\left[\frac{V_{\mathrm{t}} J_{\mathrm{m}}}{4\beta_{\mathrm{e}} D_m^2} s^2 + \left(\frac{V_{\mathrm{t}}}{4\beta_{\mathrm{e}} D_m^2} B_{\mathrm{m}} + \frac{J_{\mathrm{m}} K_{\mathrm{ce}}}{D_m^2}\right) s + 1\right]} = \frac{K_{\mathrm{q}}/D_{\mathrm{m}}}{\left(\frac{s^2}{w_h^2} + \frac{2\zeta_h}{w_h} s + 1\right)} \tag{8}$$

$$w_h = \sqrt{\frac{4\beta_{\mathrm{e}} D_{\mathrm{m}}^2}{V_{\mathrm{t}} J_{\mathrm{m}}^2}} \tag{9}$$

$$\zeta_h = \frac{K_{\mathrm{ce}}}{D_{\mathrm{m}}} \sqrt{\frac{\beta_{\mathrm{e}} J_{\mathrm{m}}}{V_{\mathrm{t}}}} + \frac{B_{\mathrm{m}}}{4D_{\mathrm{m}}} \sqrt{\frac{V_{\mathrm{t}}}{\beta_{\mathrm{e}} J_{\mathrm{m}}}} \tag{10}$$

$$K_{\mathrm{ce}} = K_{\mathrm{c}} + C_{\mathrm{m}} \tag{11}$$

Simultaneously, with Equations (6) and (8), the transfer function between the θ_{m} and T_{L} can be obtained as:

$$\frac{\theta_{\mathrm{m}}}{T_{\mathrm{m}}} = \frac{-\frac{K_{\mathrm{ce}}}{D_{\mathrm{m}}}\left(1 + \frac{V_{\mathrm{t}}}{4\beta_{\mathrm{e}} K_{\mathrm{ce}}} s\right)}{\left(\frac{s^2}{w_h^2} + \frac{2\zeta_h}{w_h} s + 1\right)} \tag{12}$$

Simultaneously, with Equations (8) and (12), the transfer function of the valve-controlled motor speed control system can be obtained, as shown in Figure 4.

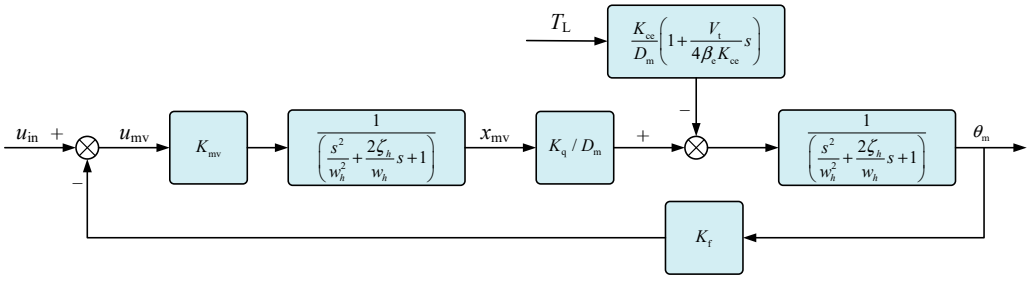

Figure 4. Block diagram of the transfer function of valve-controlled motor speed control system.

The walking of the drilling robot is driven by the left and right hydraulic motors, which are transmitted through a mechanical gear reducer mechanism for proportional reduction. The deceleration transmission process can be described as:

$$\dot{\theta}_{\mathrm{s}} = \frac{\dot{\theta}_{\mathrm{m}}}{\mathrm{n_m}} \tag{13}$$

where $\dot{\theta}_{\mathrm{s}}$ represents the output speed acting on the track after being output by the reducer; n_{m} represents the reduction ratio of the reducer.

And then, the linear speed acting on the ground of the track can be described as:

$$\begin{cases} v_{\mathrm{jL}} = \dot{\theta}_{\mathrm{s}} R_{\mathrm{sL}} \\ v_{\mathrm{jH}} = \dot{\theta}_{\mathrm{s}} R_{\mathrm{sH}} \end{cases} \tag{14}$$

Based on Figure 4 and Equation (14), the mathematical model is constituted for the speed control of the valve-controlled hydraulic motor.

3. Design of Walking Trajectory Tracking Control Strategy

3.1. Design of the State Observer Based on Improved RBF Neural Network

In the walking process of the tracked chassis for the CMDR, the driving resistance force of F_{rR}, F_{rL}, lateral resistance force of F_{yR}, F_{yL}, the centrifugal force of F_{C} (F_{Cx}, F_{Cy}), and external disturbances are not easy to acquire because of the roadway being uneven and model uncertainties. Accordingly, a state observer is designed to estimate these uncertainties based on an improved radial basis function (RBF) neural network [37], which can be used to approximate the uncertainty items. The state observer based on an improved RBF neural network can be described as:

$$F_{f1}(x) = W_1^{\mathrm{T}}\, Sn_1(x) + \varepsilon_1 \tag{15}$$

where $F_{f1}(x)$ is the uncertainty item; x is the input values of the RBF neural network; ε_1 is the approximate error; $W_1 = [w_{11}, w_{12}, w_{13}, \ldots, w_{1\mathrm{n}}]^{\mathrm{T}}$ is the connection weights among network nodes; $Sn_1(x) = [sn_{11}, sn_{12}, sn_{13}, \ldots, sn_{1\mathrm{n}}]^{\mathrm{T}}$ is the radial basis function vector.

Additionally, the RBF can be described as:

$$Sn_{1j}(x) = \exp\left(\frac{\|x - \sigma_{1j}\|_2}{2b_{1j}^2}\right) \tag{16}$$

where $\sigma_{1j}(x) = [\sigma_{11j}, \sigma_{12j}, \sigma_{13j}]^{\mathrm{T}}$ and b_{1j} are the center and width of the jth node, respectively; $\sigma_{1j} \in R$, $i = 1, 2, 3$, $j = 1, 2, \cdots, n$.

RBF networks can approximate uncertainty items by adjusting the hidden layer neurons and connection weights, and an inappropriate number of hidden layer neurons and connection weights will adversely affect the learning speed and training accuracy of the RBF network. Consequently, dynamically regulating the hidden layer neurons based on the data sample deviation from the central sample is proposed. The minimum distance can be described as:

$$l_1 = \arg\min_j \left\| x^{1i} - \sigma_{1j} \right\|_2 \tag{17}$$

where x^{1i} is the ith sample.

Additionally, the redundant neuron nodes can merge based on the node center distance among neurons. The merged neuron node center can be described as:

$$\overline{\sigma}_{1p} = \frac{\sigma_{1p} + \sigma_{1q}}{2} \tag{18}$$

where σ_{1p} and σ_{1q} are any two-neuron node centers; when $\left\|\sigma_{1p} - \sigma_{1q}\right\|_2 < \omega_1$, two neurons merge into one neuron, and ω_1 is the determination coefficient.

Assuming the W_1 is an unknown term, the $\hat{W}_1$ is the estimation value of the W_1, and the estimation error can be described as:

$$\widetilde{W}_1 = W_1 - \hat{W}_1 \tag{19}$$

Consequently, the estimation value of the uncertainty items can be described as:

$$\hat{F}_{f1}(x) = \hat{W}_1^{\mathrm{T}}\, Sn_1(x) \tag{20}$$

3.2. Design of the Walking Longitudinal Trajectory Tracking Controller

For the walking trajectory control of the WECS, the accuracy of the walking longitudinal trajectory is a prerequisite for tracking its forward displacement and ensuring accurate movement. In this process, the actual walking trajectory of the drilling robot is determined by the differential speed controlled by the left and right hydraulic motors. When the left and right tracks travel at the same speed, the drilling robot will move in a straight trajectory. Correspondingly, the ideal walking trajectory is determined by the ideal speed $v_{\mathrm{jL}}, v_{\mathrm{jH}}$ on the left and right hydraulic motors. Considering that the functions of the left and right hydraulic motors are the same, we take the left hydraulic motor as an example to establish a mathematical model. To this end, an integral sliding surface is designed to guarantee the control effectiveness and accuracy for the WECS.

$$s_c = e_{c1} + k_{c1}\int_0^t e_{c1} d\mathrm{t} \tag{21}$$

where s_c is the integral sliding surface; $k_{c1} > 0$ is the coefficient of the sliding mode control; e_{c1} is the speed error of the controlled hydraulic motor.

$$e_{c1} = v_{\mathrm{L}} - v_{\mathrm{L\,exp}} \tag{22}$$

where v_{Lexp} and v_{L} represent the expected and actual speed, respectively.

We calculate the derivative of Equation (20), and then:

$$\dot{s}_c = \dot{e}_{c1} + k_{c1} e_{c1} \tag{23}$$

In addition, the saturation function is added in the sliding mode reaching law, and then:

$$\dot{s}_c = -\varepsilon_{c1} sat(s_c) - k_{c2} s_c \tag{24}$$

where $\varepsilon_{c1} > 1$, and $k_{c2} > 0$.

If the Lyapunov function is employed as:

$$V_1 = \frac{1}{2} s_c^2 \tag{25}$$

then the derivative of the Equation (25) is described as:

$$\begin{aligned} \dot{V}_1 &= \dot{s}_c s_c = s_c\left(\dot{e}_{c1} + k_{c1} e_{c1}\right) = s_c\left(\dot{v}_{\mathrm{L}} - \dot{v}_{\mathrm{L\,exp}} + k_{c1} e_{c1}\right) \\ &= s_c\left(\dot{\theta}_{\mathrm{s}} R_{\mathrm{sL}} - \dot{v}_{\mathrm{L\,exp}} + k_{c1} e_{c1}\right) \\ &= s_c\left(g_1(x_{\mathrm{mv}}, t) u_{\mathrm{mv}} R_{\mathrm{sL}} - \dot{v}_{\mathrm{L\,exp}} + k_{c1} e_{c1}\right) \end{aligned} \tag{26}$$

The walking longitudinal trajectory tracking controller based on sliding mode control can be designed as:

$$u_{\mathrm{mv}} = \frac{1}{g(x_{\mathrm{mv}}, t) R_{\mathrm{sL}}}\left(\dot{v}_{\mathrm{L\,exp}} - k_{c1} e_{c1} - k_{c3} s_c\right) \tag{27}$$

where $k_{c3} > 0$.

Combing Equations (27) and (26),

$$\begin{aligned} \dot{V}_1 &= s_c\left(g_1(x_{\mathrm{mv}}, t)u_{\mathrm{mv}}R_{\mathrm{sL}} - \dot{v}_{\mathrm{L\,exp}} + k_{c1}e_{c1}\right) \\ &= s_c\left(\dot{v}_{\mathrm{L\,exp}} - k_{c1}e_{c1} - k_{c3}s_c - \dot{v}_{\mathrm{L\,exp}} + k_{c1}e_{c1}\right) \\ &= -k_{c3}s_c^2 \end{aligned} \tag{28}$$

where $\dot{V}_1 < 0$ indicates the system is stable.

3.3. Design of the Walking Lateral Trajectory Tracking Controller

In the actual walking movement of the drilling robot, it is easily affected by the roadway being uneven and external disturbances, leading to walking lateral errors. For the yaw angle of the drilling robot, an integral sliding surface is designed as:

$$s_a = e_{a1} + k_{a1}\int_0^t e_{a1}d\mathrm{t} \tag{29}$$

where s_a is the integral sliding surface; $k_{a1} > 0$ is the coefficient; e_{a1} is the error of the controlled hydraulic motor.

$$e_{a1} = \varphi_{\mathrm{t}} - \varphi_{\mathrm{exp}} \tag{30}$$

where φ_{exp} and φ_{t} represent the expected and actual heading angles, respectively.

We calculate the derivative of Equation (29), and then:

$$\dot{s}_a = \dot{e}_{a1} + k_{a1}e_{a1} \tag{31}$$

The saturation function is added in the sliding mode reaching law, and then:

$$\dot{s}_a = -\varepsilon_{a1}sat(s_a) - k_{a2}s_a \tag{32}$$

where $\varepsilon_{a1} > 1$, $k_{a2} > 0$.

If the Lyapunov function is designed as:

$$V_2 = \frac{1}{2}s_a^2 \tag{33}$$

then the derivative of the Equation (33) is obtained:

$$\begin{aligned} \dot{V}_2 &= \dot{s}_a s_a = s_a\left(\dot{e}_{a1} + k_{a1}e_{a1}\right) = s_a\left(\dot{\varphi}_{\mathrm{t}} - \dot{\varphi}_{\mathrm{exp}} + k_{a1}e_{a1}\right) \\ &= s_a\left(g_2(x_{\mathrm{mv}}, t)u_{\mathrm{mv}} - \dot{\varphi}_{\mathrm{exp}} + k_{a1}e_{a1}\right) \end{aligned} \tag{34}$$

The walking lateral trajectory tracking controller based on sliding mode control can be designed as:

$$u_{\mathrm{mv}} = \frac{1}{g_2(x_{\mathrm{mv}}, t)}\left(\dot{\varphi}_{\mathrm{exp}} - k_{a1}e_{a1} - k_{a3}s_a\right) \tag{35}$$

where $k_{a3} > 0$.

We combine Equations (35) and (34), and then

$$\begin{aligned} \dot{V}_2 &= s_a\left(g_2(x_{\mathrm{mv}}, t)u_{\mathrm{mv}} - \dot{\varphi}_{\mathrm{exp}} + k_{a1}e_{a1}\right) \\ &= s_a\left(\dot{\varphi}_{\mathrm{exp}} - k_{a1}e_{a1} - k_{a3}s_a - \dot{\varphi}_{\mathrm{exp}} + k_{a1}e_{a1}\right) \\ &= -k_{a3}s_a^2 \end{aligned} \tag{36}$$

where $\dot{V}_2 < 0$ represents that the system is stable.

Based on Equations (29) and (32), the adaptive sliding mode control law can be designed, and Equation (35) can be rewritten as:

$$u_{\mathrm{mv}} = \frac{1}{g_2(x_{\mathrm{mv}}, t)}\left(\hat{F}_{f1}(x) + \dot{\varphi}_{\exp} - k_{a1}e_{a1} - k_{a3}s_a - \varepsilon_{a1}sat(s_a) - k_{a2}s_a\right) \tag{37}$$

The adaptive estimation of the connection weights W_2 in the function of $F_{f1}(x)$ can be designed as:

$$\dot{\hat{W}}_2 = \frac{1}{F_{f1}(x)}s_a Sn_2(x) \tag{38}$$

If the Lyapunov function is employed as:

$$V_3 = \frac{1}{2}s_a^2 + \frac{1}{2}F_{f1}(x)\tilde{W}_2^{\mathrm{T}}\tilde{W}_2 \tag{39}$$

The derivative of Equation (39) is obtained:

$$\begin{aligned}
\dot{V}_3 &= \dot{s}_a s_a = s_a\left(\dot{e}_{a1} + k_{a1}e_{a1}\right) - F_{f1}(x)\tilde{W}_2^{\mathrm{T}}\dot{\hat{W}}_2 \\
&= s_a\left(\dot{\varphi}_{\mathrm{t}} - \dot{\varphi}_{\exp} + k_{a1}e_{a1}\right) - F_{f1}(x)\tilde{W}_2^{\mathrm{T}}\dot{\hat{W}} \\
&= s_a\left(g_2(x_{\mathrm{mv}}, t)u_{\mathrm{mv}} - \dot{\varphi}_{\exp} + k_{a1}e_{a1}\right) - \tilde{W}_2^{\mathrm{T}}s_a Sn_2(x) \\
&= s_a\left(-k_{a3}s_a - \varepsilon_{a1}sat(s_a) - k_{a2}s_a + \hat{F}_{f1}(x) - \tilde{W}_2^{\mathrm{T}}Sn_2(x)\right) \\
&= s_a(-k_{a3}s_a - \varepsilon_{a1}sat(s_a) - k_{a2}s_a)
\end{aligned} \tag{40}$$

where $\dot{V}_3 < 0$ represents that the system is stable.

3.4. The Proposed Walking Trajectory Tracking Control Strategy

To realize the precise walking trajectory tracking control of the CMDR, the control output is often executed under operating conditions to accommodate the nonlinear motion characteristics of WECS. Speed and attitude sensors and electrohydraulic proportional directional valves are used to obtain the feedback signals and output the expected controlling trajectory. Finally, the proposed walking trajectory tracking control scheme with the proposed method is shown in Figure 5. Furthermore, the proposed control strategy improves the walking trajectory tracking control accuracy and robustness, and the saturation function is used to suppress the chattering phenomenon.

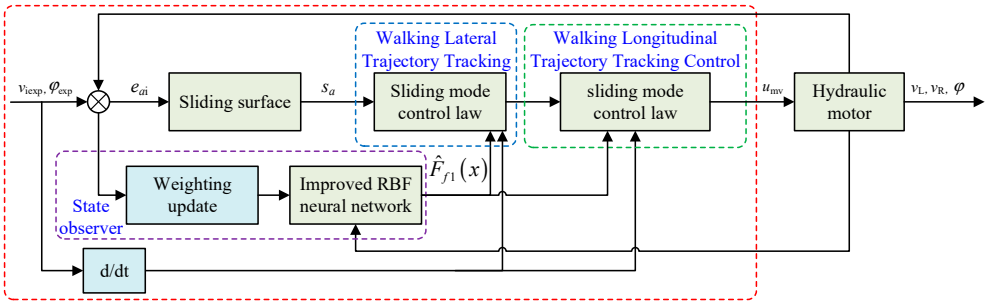

Figure 5. Schematic diagram of the walking trajectory tracking control scheme for the WECS.

4. Results and Discussion

4.1. Main Parameters

A comparison of the proportion integration differentiation (PID), SMC, and the proposed walking trajectory tracking control based on sliding mode control with the state observer (SMC-SO) was conducted for the purpose of verifying the control accuracy and effectiveness. A simulation model is established based on AMESim and MATLAB/Simulink. The main parameters of the WECS are listed in Table 1. The controller parameters of the

PID are configured as $k_P = 13$, $k_I = 8$, $k_D = 0.06$; the controller parameters of the SMC-SO are configured as $\varepsilon_{c1} = 2$, $k_{c1} = 0.6$, $k_{c2} = 8$, $k_{c3} = 8$, $\varepsilon_{a1} = 2$, $k_{a1} = 0.6$, $k_{a2} = 8$, $k_{a3} = 8$.

Table 1. Main parameters of the WECS.

Parameters	Characteristics	Values
K_q	Flow gain	1.5×10^{-10} m^3/(s·MPa)
K_c	Flow–pressure gain	4.6×10^{-5} m^3/(s·MPa)
J_m	Inertia moment	1.28 Kg/m^2
D_m	Motor displacement	1.6×10^{-4} m^3/rad
B_m	Viscous damping coefficient	0.353 N·m·s/rad
G_m	Torsional stiffness	1.2 N·m/rad
J_m	Inertia moment	1.28 Kg/m^2
ρ	Hydraulic oil density	900 Kg/m^3
β_e	bulk modulus	1.7×10^9 Pa

4.2. Simulation Results and Analysis

4.2.1. Walking Longitudinal Trajectory Tracking and Analysis

Figure 6 illustrates a comparison of the PID, SMC, and SMC-SO methods in tracking step signal to analyze the walking longitudinal tracking performance. Figure 6a shows that the steady-state time of the PID, SMC, and SMC-SO is 2.07 s, 0.87 s, and 0.58 s, respectively. Figure 6b shows that the X-direction trajectory tracking average absolute errors of the PID, SMC, and SMC-SO are 12.66 mm, 8.84 mm, and 7.86 mm, respectively, which indicates that the SMC-SO has a better tracking performance, and the longitudinal trajectory tracking average absolute error of the SMC-SO is 37.91% and 11.08% smaller than the PID and SMC, respectively. Figure 6c shows that the Y-direction trajectory tracking average absolute errors of the PID, SMC, and SMC-SO are 42.83 mm, 26.39 mm, and 17.88 mm, respectively. It can be indicated that the SMC-SO has a better tracking performance in the Y-direction trajectory, and the trajectory tracking average absolute error of the SMC-SO is 58.25% and 32.24% smaller than the PID and SMC, respectively. Figure 6d shows that the heading angle average absolute errors of the PID, SMC, and SMC-SO are 0.26 rad, 0.17 rad, and 0.11 rad, respectively. It can be shown that the heading angle can be controlled at a smaller angle than the PID and SMC, and the heading angle average absolute error of the SMC-SO is 57.69% and 35.29% smaller than the PID and SMC, respectively. Consequently, the SMC-SO has a better walking longitudinal trajectory tracking performance than the PID and SMC.

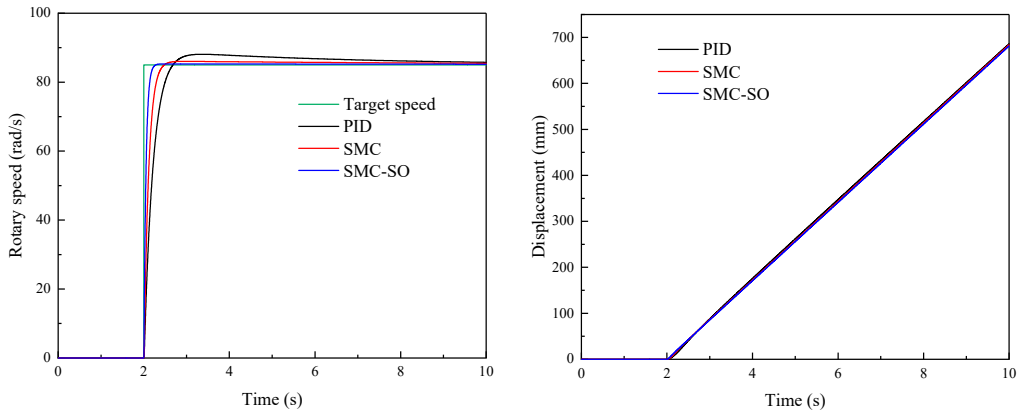

(**a**) (**b**)

Figure 6. *Cont.*

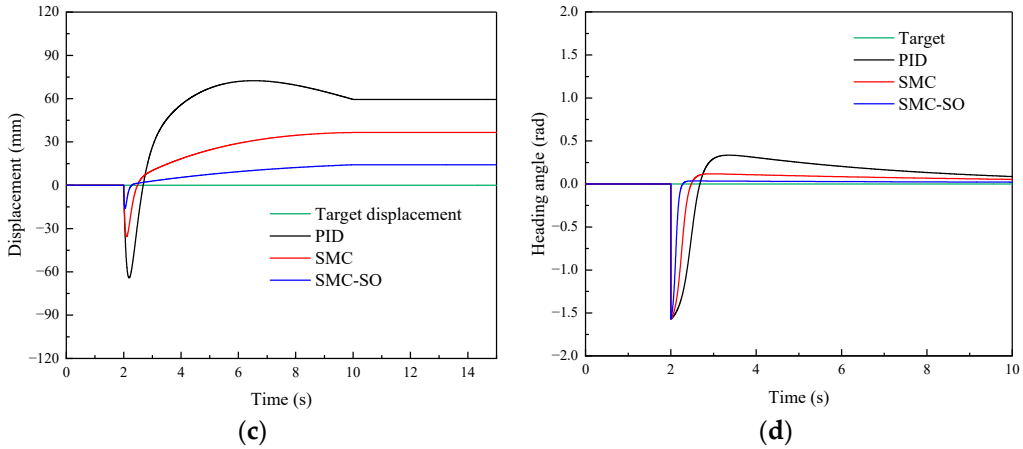

Figure 6. Comparison of the PID, SMC, and SMC-SO methods in tracking a given step signal: (**a**) the walking speed of the hydraulic motor with different methods; (**b**) the *X*-direction trajectory tracking errors with different methods; (**c**) the *Y*-direction trajectory tracking errors with different methods; (**d**) simulation results of the heading angle trajectory tracking errors with different methods.

4.2.2. Walking Lateral Trajectory Tracking Performance and Analysis

Figure 7 illustrates a comparison of the PID, SMC, and SMC-SO methods in tracking a given curve signal to analyze the walking lateral trajectory tracking performance. Figure 7a shows that the steady-state time of the PID, SMC, and SMC-SO is 0.58 s, 0.41 s, and 0.32 s, respectively. Figure 7b shows that the X-direction trajectory tracking average absolute errors of the PID, SMC, and SMC-SO are 18.36 mm, 11.65 mm, and 10.08 mm, respectively, which indicates that the SMC-SO has a better tracking performance, and the lateral trajectory tracking average absolute error of the SMC-SO is 36.54% and 13.47% smaller than the PID and SMC, respectively. Figure 7c shows that the Y-direction trajectory tracking average absolute errors of the PID, SMC, and SMC-SO are 45.94 mm, 26.66 mm, and 19.16 mm, respectively. It can be indicated that the SMC-SO has a better tracking performance in the Y-direction trajectory, and the trajectory tracking average absolute error of the SMC-SO is 58.29% and 28.13% smaller than the PID and SMC, respectively. Figure 7d shows that the heading angle average absolute errors of the PID, SMC, and SMC-SO are 0.24 rad, 0.17 rad, and 0.13 rad, respectively. It can be shown that the heading angle can be controlled at a smaller angle than the PID and SMC, and the heading angle average absolute error of the SMC-SO is 45.83% and 23.52% smaller than the PID and SMC, respectively. Based on these simulation results, the designed SMC-SO can improve the walking trajectory tracking control performance, which has a strong robustness to reject the disturbance.

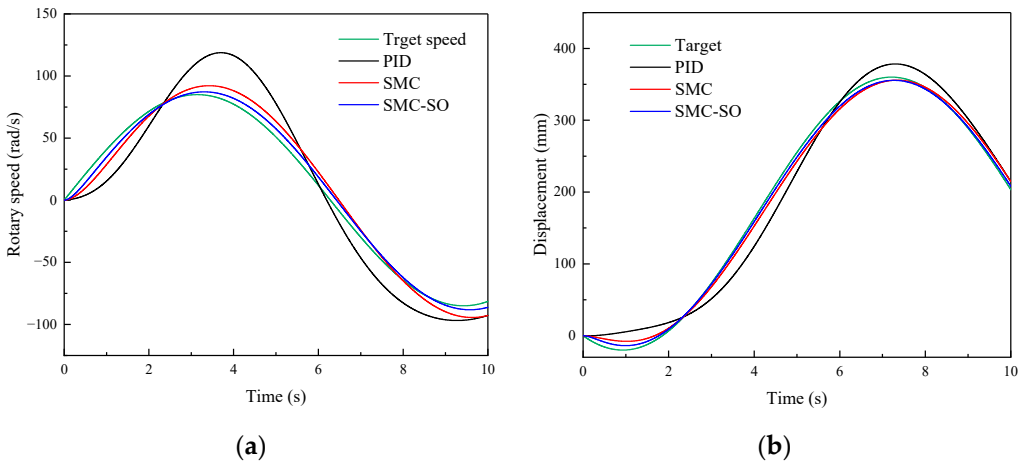

Figure 7. *Cont.*

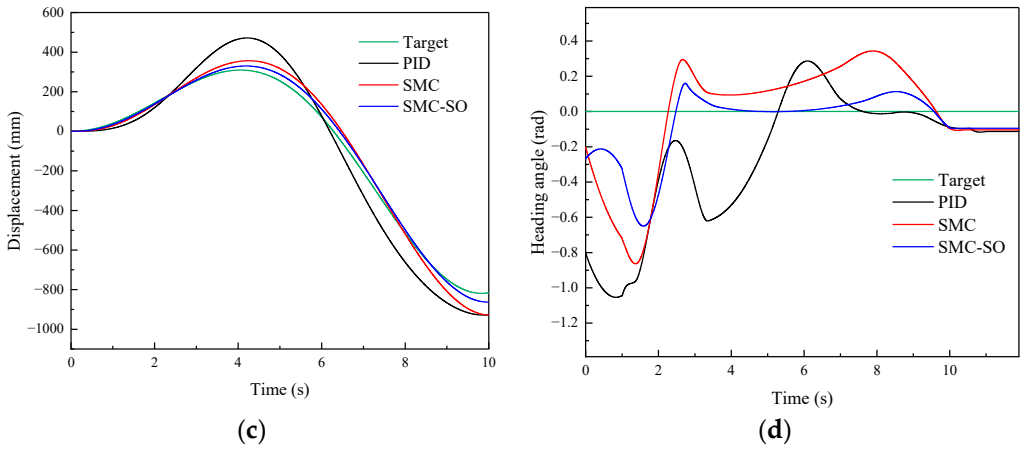

Figure 7. Comparison of the PID, SMC, and SMC-SO methods in tracking a given curve signal: (**a**) the walking speed of the hydraulic motor with different methods; (**b**) the *X*-direction trajectory tracking errors with different methods; (**c**) the *Y*-direction trajectory tracking errors with different methods; (**d**) simulation results of the heading angle trajectory tracking errors with different methods.

4.3. Experimental Results and Analysis

4.3.1. Experimental Platform of the WECS

Figure 8 shows the experimental platform for validating the designed walking trajectory tracking controller for the WECS. The designed walking trajectory tracking controller was employed utilizing PLC 1511C, including speed and attitude sensors information acquisition, electrohydraulic proportional directional valve signal output, proposed method calculating, and the sampling frequency of the speed tracking loop is 1 kHz. Additionally, the steering speed is a constant speed when conducting testing experiments, and the walking trajectory tracking performance tests were carried out to validate the practicability and effectiveness of the designed controller for the WECS.

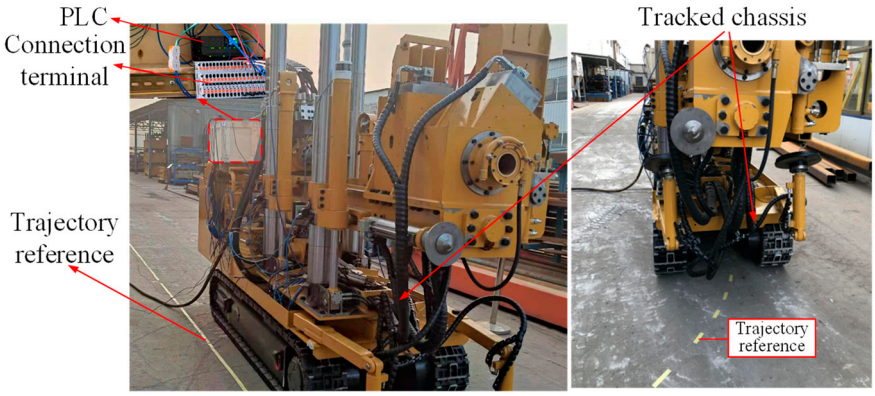

Figure 8. Experimental platform of the DTAAS.

4.3.2. Walking Longitudinal Trajectory Tracking Performance Verification

To verify the walking longitudinal trajectory tracking performance of the proposed SMC-SO method for the WECS, Figure 9 illustrates a comparison of the PID, SMC, and SMC-SO methods in tracking a given straight line signal. Figure 9a shows that the steady-state time of the PID, SMC, and SMC-SO for the walking speed is 2.11 s, 1.07 s, and 0.93 s, respectively. Figure 9b shows that the X-direction trajectory tracking average absolute errors of the PID, SMC, and SMC-SO are 16.37 mm, 12.14 mm, and 10.23 mm, respectively, which indicates that the SMC-SO has a better tracking performance. The longitudinal trajectory tracking average absolute error of the SMC-SO is 10.23 mm, which is 37.51%, 15.73% less than the PID and SMC. Figure 9c shows that the Y-direction trajectory tracking average

absolute errors of the PID, SMC, and SMC-SO are 26.91 mm, 15.95 mm, and 11.59 mm, respectively. It can be indicated that the SMC-SO has a better tracking performance in the Y-direction trajectory, and the trajectory tracking average absolute error of the SMC-SO is 56.93% and 15.22% smaller than the PID and SMC, respectively. Figure 9d shows that the heading angle average absolute errors of the PID, SMC, and SMC-SO are 0.29 rad, 0.18 rad, and 0.14 rad, respectively. It can be shown that the heading angle can be controlled at a smaller angle than the PID and SMC, and the heading angle average absolute error of the SMC-SO is 51.72% and 22.22% smaller than the PID and SMC, respectively. Therefore, the proposed SMC-SO can further improve the walking longitudinal trajectory tracking performance.

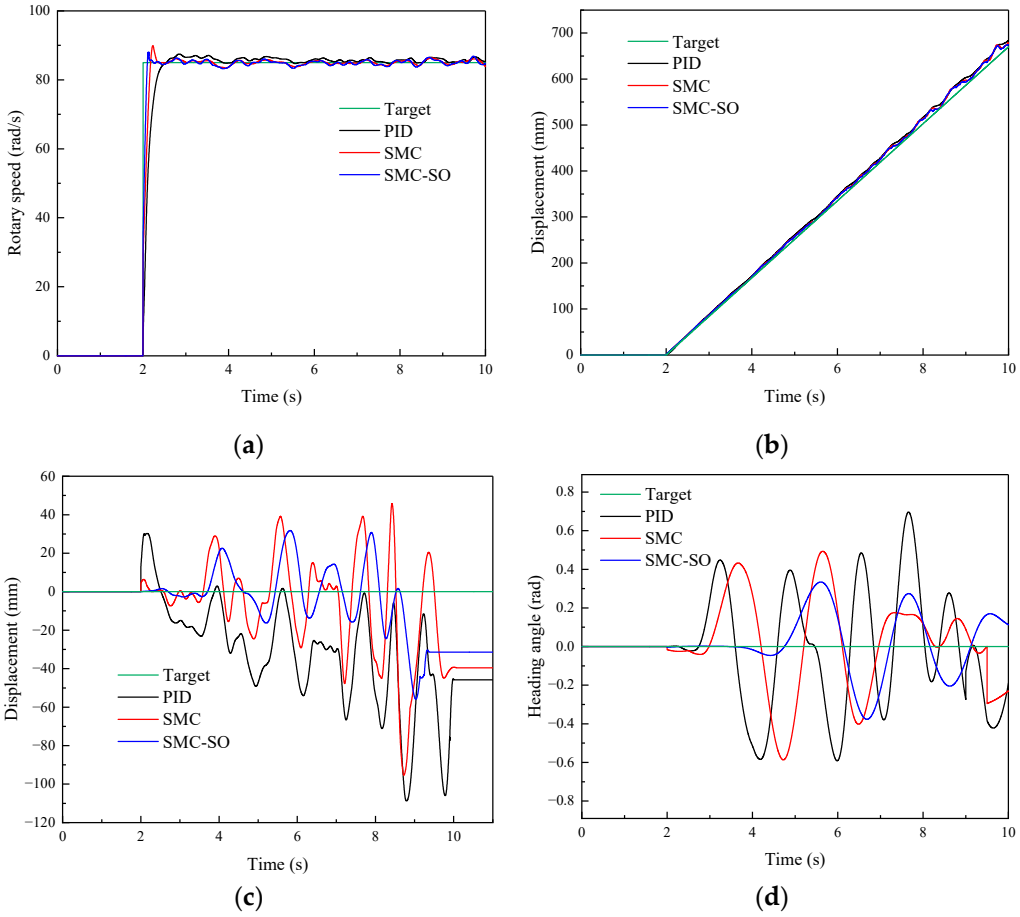

Figure 9. Comparison of the PID, SMC, and SMC-SO methods in tracking a given straight line signal: (**a**) the walking speed of the hydraulic motor with different methods; (**b**) the *X*-direction trajectory tracking errors with different methods; (**c**) the *Y*-direction trajectory tracking errors with different methods; (**d**) experimental results of the heading angle trajectory tracking errors with different methods.

4.3.3. Walking Lateral Trajectory Tracking Performance Verification

To verify the walking lateral trajectory tracking performance of the proposed SMC-SO method for the WECS, Figure 10 illustrates a comparison of the PID, SMC, and SMC-SO methods in tracking a given curve line signal. Figure 10a shows that the steady-state time of the PID, SMC, and SMC-SO is 0.77 s, 0.54 s, and 0.48 s, respectively. Figure 10b shows that the X-direction trajectory tracking average absolute errors of the PID, SMC, and SMC-SO are 27.31 mm, 16.27 mm, and 14.59 mm, respectively, which indicates that the SMC-SO has a better tracking performance, and the lateral trajectory tracking average absolute error of the SMC-SO is 46.57% and 10.33% smaller than the PID and SMC, respectively. Figure 10c shows that the Y-direction trajectory tracking average absolute errors of the

PID, SMC, and SMC-SO are 46.42 mm, 28.97 mm, and 22.34 mm, respectively, which can indicate that the SMC-SO has a better tracking performance in the Y-direction trajectory. The lateral trajectory tracking average absolute error of the SMC-SO is 22.34 mm, which is 51.87% and 22.89% less than the PID and SMC. Figure 10d shows that the heading angle average absolute errors of the PID, SMC, and SMC-SO are 0.36 rad, 0.21 rad, and 0.19 rad, respectively. It can be shown that the heading angle can be controlled at a smaller angle than the PID and SMC, and the heading angle average absolute error of the SMC-SO is 47.22% and 9.52% smaller than the PID and SMC, respectively. Therefore, it can be indicated that the proposed SMC-SO has a better walking lateral trajectory tracking performance than the PID and SMC, which can effectively improve the walking trajectory tracking capability of the WECS.

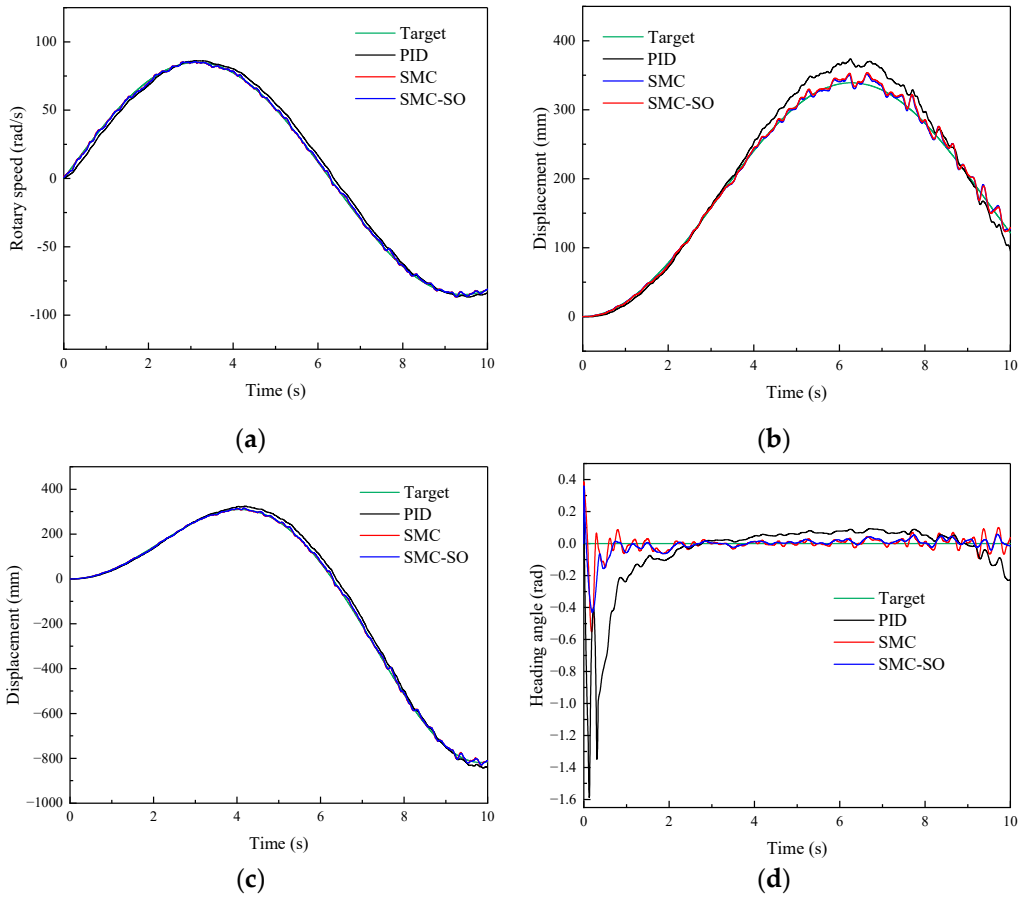

Figure 10. Comparison of the PID, SMC, and SMC-SO methods in tracking a given curve line signal: (**a**) the walking speed of the hydraulic motor with different methods; (**b**) the *X*-direction trajectory tracking errors with different methods; (**c**) the *Y*-direction trajectory tracking errors with different methods; (**d**) experimental results of the heading angle trajectory tracking errors with different methods.

5. Conclusions

A walking trajectory tracking control scheme for the WECS using the SMC-SO is proposed. Targeting the walking trajectory tracking deviation of the WECS for the CMDR, an SMC-SO method using a state observer, was proposed to realize system rapid response characteristics and disturbance rejection performance. Then, the improved RBF is employed to approximate the uncertainties. In addition, the saturation function is used to reduce the sliding mode chattering phenomenon. Furthermore, simulation and experimental results indicate that the proposed method has a better walking trajectory tracking performance and stronger robustness than the comparison methods. Meanwhile, the walking longitudinal

and lateral trajectory performance of the SMC-SO is verified by the comparative simulation and experimental results under different operating conditions. In the future, the proposed method could also be applied to speed or position tracking control in other systems, such as the electrohydraulic rotary system of a geological exploration drilling rig, electrohydraulic drive system of the heavy mobile equipment, etc. Additionally, a more detailed chattering suppression method, disturbance rejection control approach, and more detailed trajectory tracking error analysis strategy could be explored in future research.

Author Contributions: Conceptualization, J.G. and S.H.; methodology, J.G.; software, S.H.; validation, J.G. and S.H.; formal analysis, J.D., D.W. and H.Y.; investigation, J.G. and C.T.; resources, Z.W. and L.S.; data curation, S.H., J.D. and D.W.; writing—original draft preparation, J.G. and L.S.; writing—review and editing, J.G. and L.S.; visualization, S.H.; supervision, C.T. and L.S.; project administration, Z.W.; funding acquisition, J.G. and Z.W. All authors have read and agreed to the published version of the manuscript.

Funding: This research was supported in part by the following research projects: National Natural Science Foundation of China (no. 52304184), and Jiangsu Funding Program for Excellent Postdoctoral Talent (no. 2022ZB517).

Data Availability Statement: The data are contained within the article.

Conflicts of Interest: The authors declare no conflicts of interest.

References

1. Wu, S.-K.; Zhang, J.-W.; Song, Z.-X.; Fan, W.-B.; Zhang, Y.; Dong, X.-K.; Zhang, Y.-J.; Kan, B.-H.; Chen, Z.-S.; Zhang, J.-T. Review of the development status of rock burst disaster prevention system in China. *J. Cent. South Univ.* **2023**, *30*, 3763–3789. [CrossRef]
2. He, X.-Q.; Zhou, C.; Song, D.-Z.; Li, Z.-L.; Cao, A.-Y.; He, S.-Q.; Khan, M. Mechanism and monitoring and early warning technology for rockburst in coal mines. *Int. J. Miner. Metall. Mater.* **2021**, *28*, 1097–1111. [CrossRef]
3. Ma, N.; Zhang, W.; Li, J.; Lian, X.; Ren, J. Analysis and evaluation of essential factors for rock burst mechanism. *J. Min. Sci. Technol.* **2021**, *6*, 651–658.
4. Si, L.; Wang, Z.; Li, J.; Wei, D.; Zhao, S. A novel positioning method of anti-punching drilling robot based on the fusion of multi-IMUs and visual image. *ISA Trans.* **2023**, *137*, 730–746. [CrossRef] [PubMed]
5. Yuan, L. Risk identification, monitoring and early warning of typical coal mine dynamic disasters during the 13th Five-Year Plan period. *J. Min. Sci. Technol.* **2021**, *6*, 1–8.
6. Borrell, A.M.; Puig, V.; Sename, O. Fixed-structure parameter-dependent state feedback controller: A scaled autonomous vehicle path-tracking application. *Control Eng. Pract.* **2024**, *147*, 105911. [CrossRef]
7. Sun, J.; Yao, J.; Jia, Y.; Yao, F.; Shi, W. Nonlinear model predictive control for trajectory-planning and tracking based on tilting technology to achieve vehicle obstacle avoidance. *Veh. Syst. Dyn.* **2024**, 1–21. [CrossRef]
8. Shao, X.; Fan, Y.; Shao, J.; Sun, G. Improved active disturbance rejection control with the optimization algorithm for the leg joint control of a hydraulic quadruped robot. *Meas. Control* **2023**, *56*, 1359–1376. [CrossRef]
9. Gao, B.; Guan, H.; Shen, W.; Ye, Y. Application of the gray wolf optimization algorithm in active disturbance rejection control parameter tuning of an electro-hydraulic servo unit. *Machines* **2022**, *10*, 599. [CrossRef]
10. Yang, W.; Ding, S.; Ding, C. Fast Supertwisting Sliding Mode Control With Antipeaking Extended State Observer for Path-Tracking of Unmanned Agricultural Vehicles. *IEEE Trans. Ind. Electron.* **2024**, 1–10. [CrossRef]
11. Iqbal, J.; Ullah, M.I.; Khan, A.A.; Irfan, M. Towards sophisticated control of robotic manipulators: An experimental study on a pseudo-industrial arm. *Stroj. Vestn.-J. Mech. Eng.* **2015**, *61*, 465–470. [CrossRef]
12. Guo, K.; Li, M.; Shi, W.; Pan, Y. Adaptive tracking control of hydraulic systems with improved parameter convergence. *IEEE Trans. Ind. Electron.* **2021**, *69*, 7140–7150. [CrossRef]
13. Gao, Q. Nonlinear adaptive control with asymmetric pressure difference compensation of a hydraulic pressure servo system using two high speed on/off valves. *Machines* **2022**, *10*, 66. [CrossRef]
14. Shen, W.; Wang, J. An integral terminal sliding mode control scheme for speed control system using a double-variable hydraulic transformer. *ISA Trans.* **2022**, *124*, 386–394. [CrossRef] [PubMed]
15. Anjum, M.B.; Khan, Q.; Ullah, S.; Hafeez, G.; Fida, A.; Iqbal, J.; Albogamy, F.R. Maximum power extraction from a standalone photo voltaic system via neuro-adaptive arbitrary order sliding mode control strategy with high gain differentiation. *Appl. Sci.* **2022**, *12*, 2773. [CrossRef]
16. Khan, M.F.; ul Islam, R.; Iqbal, J. Control strategies for robotic manipulators. In Proceedings of the 2012 International Conference of Robotics and Artificial Intelligence, Rawalpindi, Pakistan, 22–23 October 2012; IEEE: Piscataway, NJ, USA, 2012; pp. 26–33.
17. Lee, H.; Utkin, V.I. Chattering suppression methods in sliding mode control systems. *Annu. Rev. Control* **2007**, *31*, 179–188. [CrossRef]

18. Wan, Z.; Fu, Y.; Liu, C.; Yue, L. Sliding Mode Control Based on High Gain Observer for Electro-Hydraulic Servo System. *J. Electr. Comput. Eng.* **2023**, *2023*, 7932117. [CrossRef]
19. Nguyen, M.H.; Dao, H.V.; Ahn, K.K. Extended sliding mode observer-based high-accuracy motion control for uncertain electro-hydraulic systems. *Int. J. Robust Nonlinear Control* **2023**, *33*, 1351–1370. [CrossRef]
20. Wang, Y.; Zhao, J.; Ding, H.; Zhang, H. Output feedback control of electro-hydraulic asymmetric cylinder system with disturbances rejection. *J. Frankl. Inst.* **2021**, *358*, 1839–1859. [CrossRef]
21. Hu, C.; Chen, Y.; Wang, J. Fuzzy observer-based transitional path-tracking control for autonomous vehicles. *IEEE Trans. Intell. Transp. Syst.* **2020**, *22*, 3078–3088. [CrossRef]
22. Hu, Y.; Wang, H. Robust tracking control for vehicle electronic throttle using adaptive dynamic sliding mode and extended state observer. *Mech. Syst. Signal Process.* **2020**, *135*, 106375. [CrossRef]
23. Xiaodong, J.; Yuanyuan, Q.; Shichen, F.; Minjun, Z.; Miao, W. Path tracking of mining boom road-header using SVD-Unscented Kalman Filtering. *J. Min. Sci. Technol.* **2022**, *7*, 354–363.
24. Taghavifar, H.; Shojaei, K. Adaptive robust control algorithm for enhanced path-tracking performance of automated driving in critical scenarios. *Soft Comput.* **2023**, *27*, 8841–8854. [CrossRef]
25. Xi, R.-D.; Ma, T.-N.; Xiao, X.; Yang, Z.-X. Design and implementation of an adaptive neural network observer–based backstepping sliding mode controller for robot manipulators. *Trans. Inst. Meas. Control* **2024**, *46*, 1093–1104. [CrossRef]
26. Jo, A.; Lee, H.; Seo, D.; Yi, K. Model-reference adaptive sliding mode control of longitudinal speed tracking for autonomous vehicles. *Proc. Inst. Mech. Eng. Part D J. Automob. Eng.* **2023**, *237*, 493–515. [CrossRef]
27. Zhang, Z.; Guo, Y.; Gong, D.; Zhu, S. Hybrid extended state observer-based integral sliding mode control of the propulsion for a hydraulic roofbolter. *Control Eng. Pract.* **2022**, *126*, 105260. [CrossRef]
28. Zang, W.; Zhang, Q.; Shen, G.; Fu, Y. Extended sliding mode observer based robust adaptive backstepping controller for electro-hydraulic servo system: Theory and experiment. *Mechatronics* **2022**, *85*, 102841. [CrossRef]
29. Yang, X.; Yao, J.; Deng, W. Output feedback adaptive super-twisting sliding mode control of hydraulic systems with disturbance compensation. *ISA Trans.* **2021**, *109*, 175–185. [CrossRef] [PubMed]
30. Yao, Z.; Liang, X.; Zhao, Q.; Yao, J. Adaptive disturbance observer-based control of hydraulic systems with asymptotic stability. *Appl. Math. Model.* **2022**, *105*, 226–242. [CrossRef]
31. Razmjooei, H.; Palli, G.; Nazari, M. Disturbance observer-based nonlinear feedback control for position tracking of electro-hydraulic systems in a finite time. *Eur. J. Control* **2022**, *67*, 100659. [CrossRef]
32. Truong, H.V.A.; Nam, S.; Kim, S.; Kim, Y.; Chung, W.K. Backstepping-Sliding-Mode-Based Neural Network Control for Electro-Hydraulic Actuator Subject to Completely Unknown System Dynamics. *IEEE Trans. Autom. Sci. Eng.* **2023**, 1–15. [CrossRef]
33. Palli, G.; Strano, S.; Terzo, M. A novel adaptive-gain technique for high-order sliding-mode observers with application to electro-hydraulic systems. *Mech. Syst. Signal Process.* **2020**, *144*, 106875. [CrossRef]
34. Xiong, G.-M.; Lu, H.; Guo, K.-H.; CHEN, H.-Y. Research on trajectory prediction of tracked vehicles based on real time slip estimation. *Acta Armamentarii* **2017**, *38*, 600.
35. Lu, J.; Zhang, D.; Huang, G.; Li, X.; Gao, H.; Yin, G. Effects of loading rate on the compound dynamic disaster in deep underground coal mine under true triaxial stress. *Int. J. Rock Mech. Min. Sci.* **2020**, *134*, 104453. [CrossRef]
36. Gu, J.; Shen, C.; Zhang, C.; Wu, H.; Wei, D.; Si, L.; Wang, Z. Electrohydraulic proportional position and pressure loading control utilizing a state perception and processing method. *ISA Trans.* **2023**, *143*, 647–665. [CrossRef]
37. Lin, S.-C.; Chen, Y.-Y. RBF-network-based sliding mode control. In Proceedings of the IEEE International Conference on Systems, Man and Cybernetics, San Antonio, TX, USA, 2–5 October 1994; IEEE: Piscataway, NJ, USA, 1994; pp. 1957–1961.